Fabricating an electroactive injectable hydrogel based on pluronic-chitosan/aniline-pentamer containing angiogenic factor for functional repair of the hippocampus ischemia rat model

Melika Nourbakhsh, Payam Zarrintaj, Seyed Hassan Jafari, Sayed Masoud Hosseini, Shayan Aliakbari, Hamid Gholami Pourbadie, Nima Naderi, Mohammad Ismail Zibaii, Saman Seyed Gholizadeh, Joshua D. Ramsey, et al.

Fabricating an Electroactive Injectable Hydrogel Based on Pluronic-Chitosan/Aniline-Pentamer Containing Angiogenic Factor for Functional Repair of the Hippocampus Ischemia Rat Model

Melika Nourbakhsh[1#], Payam Zarrintaj[2#], Seyed Hassan Jafari[1*], Sayed Masoud Hosseini[3,4], Shayan Aliakbari[3], Hamid Gholami Pourbadie[3], Nima Naderi[4], Mohammad Ismail Zibaii[5], Saman Seyed Gholizadeh[6], Joshua D. Ramsey[2], Sabu Thomas[7], Mehdi Farokhi[8*], Mohammad Reza Saeb[9*]

1. School of Chemical Engineering, College of Engineering, University of Tehran, Tehran, Iran
2. School of Chemical Engineering, Oklahoma State University, Stillwater, OK 74078, United States
3. Department of Physiology and Pharmacology, Pasteur Institute of Iran, Tehran, Iran
4. Department of Pharmacology and Toxicology, School of Pharmacy, Shahid Beheshti University of Medical Sciences, Tehran, Iran
5. Laser and Plasma Research Institute, Shahid Beheshti University, Tehran, Iran
6. Department of Microbiology, College of Basic Science, Shiraz Branch, Islamic Azad University, Shiraz, Iran
7. School of Chemical Sciences, M G University, Kottayam 686560, Kerala, India
8. National Cell Bank of Iran, Pasteur Institute of Iran, P.O. Box 1316943551, Tehran, Iran
9. Departments of Resin and Additives, Institute for Color Science and Technology, P.O. Box 16765-654, Tehran, Iran

[#]These authors contributed equally to this work.

Corresponding authors:

Seyed Hassan Jafari; E-mail: shjafari@aut.ac.ir

Mehdi Farokhi: m_farokhi@pasteur.ac.ir

Mohammad Reza Saeb: E-mail: saeb-mr@icrc.ac.ir

Abstract

The hippocampus, a critical cerebral region involved in learning and memory formation, is especially vulnerable to ischemic defect. Here, we developed an injectable electroactive hydrogel based on pluronic-chitosan/aniline-pentamer with proper conductivity around 10^{-4} S/cm to achieve the functional repair of the hippocampus following the ischemic defect. FTIR, DSC, and TGA measurements were performed to assess the chemical structure and thermal stability of the synthesized hydrogel. Aniline pentamer decreased the swelling capacity, degradation, and drug release rate. Further, contact angle, melting point, and gelation time of hydrogels were enhanced by addition of aniline oligomer. Moreover, it endowed the on-demand electro-responsive drug release. Injectability of hydrogel was evaluated by rheometry, exhibiting proper gelling time at the body temperature. The ionic/electrical conductivity and desired *in vitro* biocompatibility with PC12 cells were also achieved. Injection of VEGF-loaded electroactive hydrogel in the hippocampal ischemic animal model resulted in decreased infarction volume, improved hippocampal dependent learning, and memory performance. Taken all together, the results confirmed that fabricated injectable hydrogel would be a suitable candidate for ischemic defect treatment and can lead to new horizons to treat neurological disorders.

Keywords: Chitosan; Pluronic; Aniline oligomer; Injectable hydrogel; VEGF; Hippocampal ischemia

1. Introduction

The hippocampus, a complex brain structure, is placed deep into the temporal lobe with the ability to regulate the hypothalamic activities [1], emotional behavior [2], and spatial navigation [3]. Many defects like ischemia and traumatic brain injury cause injury to the hippocampus, which can be partly restricted into one or some subareas [4]. For this, investigating the functionality of the hippocampus attracts significant attention. The hippocampus is also known as the region in the brain that is able to regenerate even in adulthood [5]. Any damage in different portions of the hippocampus alters the rate of neurogenesis, which causes anterograde amnesia for declarative memory and affects the relational and declarative memories formation [6]. Neurogenesis in adults usually occurs after any external stimulation that affects the functions of neurons. For the hippocampal regeneration, many therapeutic strategies, including the administration of antidepressant drugs, deep stimulation of the brain, and exercise, have been performed [7]. Recently, the achievements in applicable tools and increasing the knowledge about the process of nerve regeneration opened a new avenue to develop better strategies for optimal neuronal repair. For instance, by using nerve tissue engineering, it is possible to combine cells and materials in a substrate to provide proper support for the regeneration of nerve injuries [8-10]. Among various scaffolds that support the neural repair, hydrogels exhibit the better neural regeneration [11, 12]. Hydrogels are permeable to oxygen/nutrition and have low interfacial tensions that bypass the barriers against migrations of cells into the surrounding tissues [13]. Moreover, hydrogels are capable to deliver the encapsulated reagents e.g., growth factors, drugs, and cells to promote the desired function [14-18]. Among the wide range of hydrogels, electroactive hydrogels formed by conductive polymers are more used for nerve tissue engineering [19-21]. The need for using electroconductive polymers for better stimulations neural regenerate raises from the inherent electrical properties of nerve cells. Electroactive biomaterials have been introduced as a new generation of smart systems [22, 23]. The redox switching behavior of conductive polymers causes to control the drug release rate using electrical stimulation [24, 25]. Scrutinized survey on tissues mechanical and electrical properties lead us to select the proper material for tissue regeneration [26, 27]. It is obvious that the brain modulus is ~10^4 Pa [28], and brain tissue conductivity has been reported ~10^{-3} to 10^{-4} S/cm [29] (Figure 1). Here, we fabricated an injectable hydrogel based on Pluronic-chitosan (CS)/aniline-pentamer. Pluronic (poly (ethylene oxide)-b-poly(propylene oxide)-b-poly(ethylene oxide)) as a tri-block

copolymer contains hydrophilic and hydrophobic segments which hydrophobic interaction above lower critical solution temperature (LCST) between poly(propylene oxide) segments results in gel formation *in suit* (thermosensitive behavior) [30].

CS is a common polysaccharide produced by the deacetylation of chitin and formed by glycoside reactions between glucosamine and N-acetylglucosamine subunits. The primary amino groups of CS make them easily dissolve in acidic solutions and thus facilitate chemical modification [31-33]. CS as a natural polymer has been widely used in tissue engineering because of its acceptable interaction with cells and tissues [34-36]. It has been reported that the conductive matrix of CS increase the neural cell activities and regeneration [37-39]. Various type of conductive materials have been used in tissue engineering [40]. However, some conducting materials due to the arduous synthesis method, poor processability, and prolonged maintenance in the body resulted in some difficulties during their usage [41, 42]. Overcoming such problem, conductive oligomers have been utilized to fabricate the bio conductive materials [43]. In this study, CS was electro-activated using aniline-pentamer segments because aniline oligomer is highly stable, cost-effectiveness, biodegradable, and capable of switching between resistive and conductive states by doping/dedoping process [43, 44]. Furthermore, to improve the recovery of ischemia imperfection of the hippocampus, vascular endothelial growth factor (VEGF) was used. Localized VEGF delivery has proven greatly advantageous for tissue regeneration by enhancing neovascularization [45-47]. VEGF also act as a protein with neuroprotection and neurogenesis properties. VEGF has a central role in the reduction of infarct size, improving neurological performance, and angiogenesis promotion [48]. However, most of the growth factors are water-soluble, which are possible to rapidly diffuse into the culture media [49]. It was reported that reported that by intracerebral injection of alginate hydrogels, it was possible to control the release of VEGF in a rodent model of stroke. The alginate hydrogels containing VEGF protected the neuronal cells neurological and anatomically, which made this hydrogel promising for clinical treatment of stroke and CNS disease [50]. Here, we attempted to develop an ischemia hippocampus animal model to evaluate the effectiveness of pluronic–CS/aniline oligomer in repairing CNS. Based on our knowledge, it can be claimed that this study is the first research work of the hippocampus neurogenesis using a novel VEGF-loaded conductive injectable hydrogel.

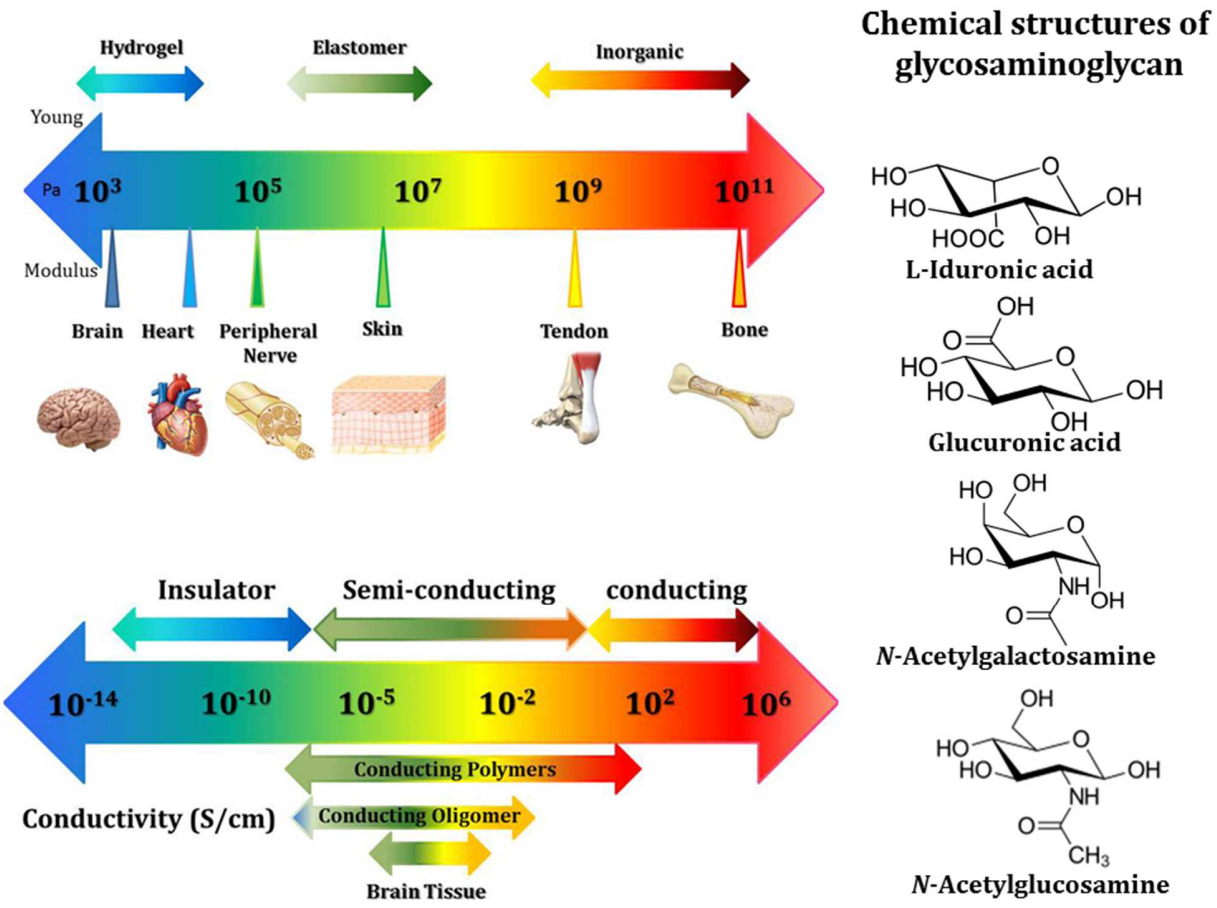

Figure 1. Comparison of tissues mechanical and electrical properties with various types of materials and composition of the glycosaminoglycans. The brain is known as a soft tissue which the selected material to regenerate the ischemic brain should be mimic its mechanical properties. Moreover, brain conductivity is similar to semiconducting materials. Selected material chemistry should be resembled ECM to mimic the ECM properties.

2. Material and methods

2.1 Materials

Dimethyl sulfoxide (DMSO), dimethyl formamide (DMF), carbodiimide crosslinking agent (N, N-di cyclohexyl carbodiimide (DCC) and N-hydroxysuccinimide (NHS)), ammonium peroxidisulfate (APS), camphor sulfonic acid, and succinic anhydride were purchased from Merck. Medium molecular weight CS, 4-aminodiphenylamine, benzene-1,4-diamine, Pluronic F127, 3-(4,5-dimethylthiazol-2-yl)- 2,5-diphenyl tetrazolium bromide (MTT), fetal bovine serum

(FBS), Dulbecco Modified Eagle's Medium (DMEM), streptomycin, triphenyltetrazolium chloride, and penicillin were purchased from Sigma-Aldrich Company.

2.2 Experimental methods

2.2.1 NHS-capped Aniline Pentamer Synthesis

4-Aminodiphenylamine was reacted with succinic anhydride to achieve the aniline dimer with carboxylic end group. To achieve the aniline pentamer (AP) with carboxylic end groups benzene-1,4-diamine was mixed with carboxylic-capped aniline dimer solution and APS was poured to the mixture slowly to proceed the reaction. Reacting of aniline pentamer with CS necessitated activation of AP end groups. In this regards, NHS/DCC was added to the carboxyl-capped AP to achieve the AP with NHS activated end groups [51].

2.2.2 Chitosan graft-NHS capped AP synthesis route

CS amine groups reacted with carboxylic end groups of AP using carbodiimide reaction. About 0.5 gr of CS was dissolved in 20 ml camphor sulfonic acid. Also, 0.1 gr NHS-capped-AP were dissolved in 5 ml DMSO. Subsequently, the two solutions were mixed and stirred for 24h at 50 °C under the nitrogen atmosphere [31].

2.2.3 Synthesis of CS-graft- NHS capped AP / Pluronic F127

Carboxylated Pluronic was synthesized with succinic anhydride dimethylaminopyridine (DMAP) and triethylamine which was dissolved and stirred overnight. The solvent was removed and diethyl ether was used to precipitate residue. Finally, activated Pluronic was achieved with product vacuum drying. The CS-AP was reacted with 0.5, 0.25, and 0.12 gr activated-Pluronic using carbodiimides reaction (EDC/NHS) to achieve the CS-AP-Pluronic (CAP1, CAP2, and CAP3).

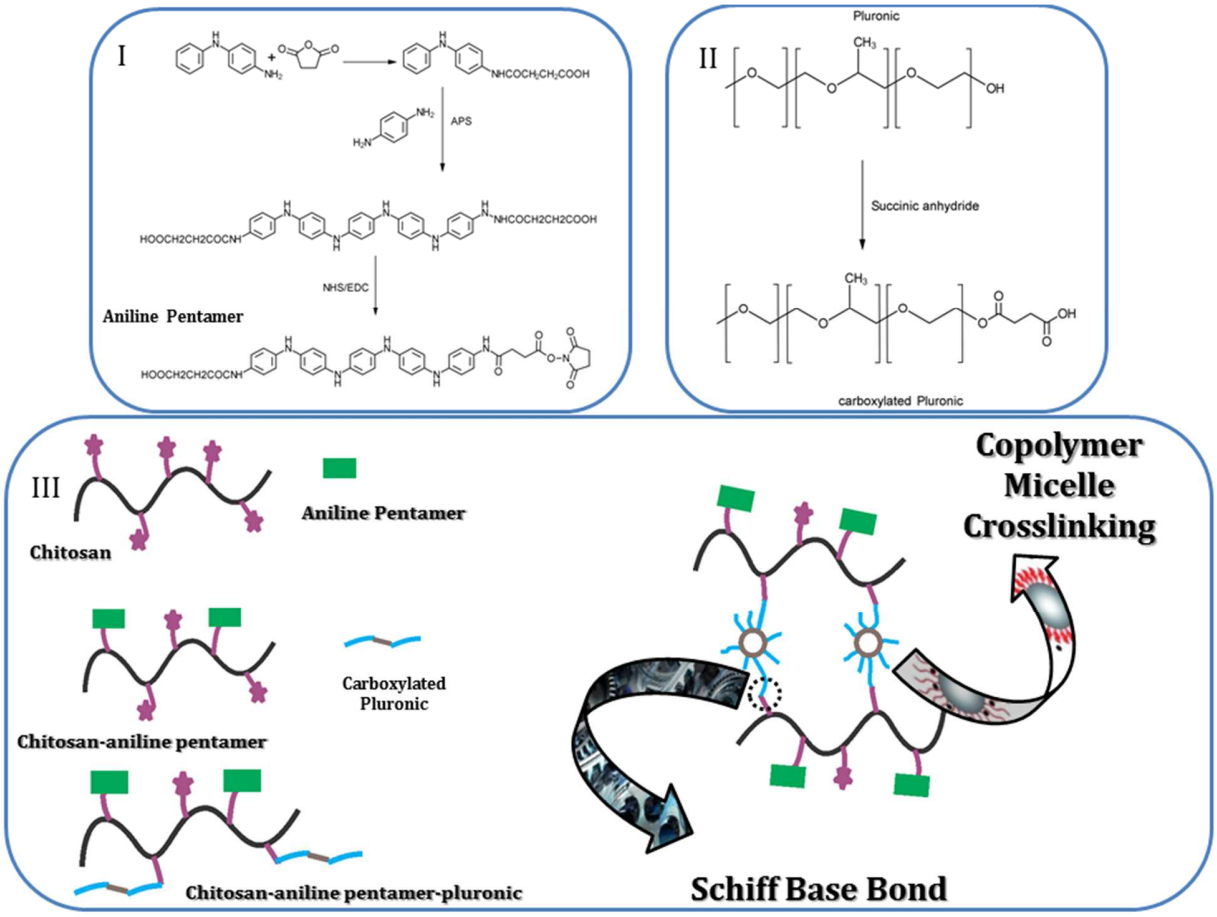

Figure 2. Chitosan-aniline pentamer- Pluronic synthesis route. I) synthesis carboxyl-capped AP: succinic anhydride reacted with 4-aminodiphenylamine to achieve the aniline dimer with carboxylic end groups. After that, the product was reacted with benzene-1,4-diamine and APS to obtain carboxyl-capped AP II) Pluronic hydroxyl group was activated using succinic anhydride to facilitate the reaction with chitosan, III) AP reacted with chitosan and then activated Pluronic grafted to the CS-AP. Pluronic tended to self-assembly and acted as a crosslinking agent with enhancing temperature.

2.3 Characterization and experiments

2.3.1 Fourier transformed infrared spectroscopy (FT-IR)

Chemical interaction of the component and CAP chemical structure was studied using FTIR spectra (Bruker instrument with the KBr disc, made by Germany, working in the range of 4000-600 cm^{-1} at ambient temperature).

2.3.2 Electro activity and conductivity

UV-visible (UV-Vis) was utilized to evaluate the AP transition states in doped and undoped state (Camphor sulfonic acid (CSA) was utilized to dope AP) of the copolymer with Shimadzu spectrophotometer (Kyoto, Japan). DMSO/deionized water (1:1) mixture was used to dissolve AP and the spectra of the doped and undoped AP using camphor sulfonic acid were assessed at 340 nm [52].

Cyclic voltammetry (CV) was applied to evaluate the CAP electroactivity impedance. Spectroscopy was also assessed to determine the electrochemical behavior of the samples using micro auto lab (III). Carbon paste electrode (CPE), platinum wire, and Ag/AgCl were worked as electrode, counter electrode, and reference electrode, respectively. One M HCl solution was used as medium at a scan rate of 50 mVs^{-1}. Also, EIS was done in 0.01 Hz. EIS by the neural model which consists of one capacitance and two resistors. With EIS records, Nyquist plot and conductivity properties were obtained [53].

The conductivity of the hydrogel was determined using four-probe method [54]. Pellet like shape of the sample was formed. After that, volt and amperes were applied and conductivity was calculated using the Eq. (1):

$$\sigma = \frac{1}{R}\frac{d}{S} \quad (1)$$

Where σ is conductivity, d is thickness, R is resistance, and S is area of the sample. Swollen samples were utilized to determine the ionic conductivity at different temperatures using Eq. (2):

$$\sigma = \frac{\sigma_0}{T}\exp\left(-\frac{E_a}{RT}\right) \quad (2)$$

Where, σ_0 is conductivity of sample before exposing to swelling situation, T is absolute temperature, E_a is activation energy, and R is constant (molar gas). Conductivity is a subordinate of mobility and hole concentration according to Eq. (3):

$$\sigma = q \times \mu_p \times p \quad (3)$$

Where P, μ_p, and q and are hole concentration, mobility, and electronic charge value (1.6×10^{-19} C), respectively [55, 56].

2.3.3 Gelation time and rheological characterization

The gelation time and storage modulus of hydrogels were measured using MCR 300 Anton Paar Rheometer with cylinder geometry. Temperature sweep test was done in the range of 15°C to 70°C, a frequency 0.1 Hz and strain of 1%. Time sweep experiment was conducted with a frequency 1 Hz and strain of 1% at 30 °C. Also, a dynamic frequency sweep experiment was performed (frequency ranging from 1 to 100 rad s^{-1} at shear amplitude of 0.1%).

2.3.4 Swelling/deswelling behavior of hydrogels

The swelling ratio of hydrogels with similar size and shapes was measured over a day at room temperature in distilled water (pH=7.2). First, hydrogels were freeze-dried and then were immersed in distilled water. After specified time intervals samples were taken out, and weighted after removing excess water. The swelling ratio of the sample was determined using equation (5), in which SR, W_s, W_d were swelling ratio of sample, the swollen weight of sample at specified time interval, and sample weight in dry state, respectively.

$$SR = \frac{W_s - W_d}{W_s} \times 100 \quad (4)$$

The equilibrium water content (EWC) and the rate parameter were intended according to equation (6) and (7).

$$EWC = \frac{W_e - W_d}{W_e} \times 100 \quad (5)$$

$$S_t = S_e(1 - e^{-t/\tau}) \quad (6)$$

Equation (7) is called Voigt equation, and W_e, S_t and S_e are the weight of swollen hydrogel at equilibrium state, swelling ratio at time t and equilibrium the swelling ratio.

In order to assess deswelling behavior, after hydrogels were reached swelling equilibrium, the samples were weighted immediately in specific periods. The water retention (WR) was measured from Equation (8) where W_t is the hydrogel weight at a certain time of deswelling

$$WR = \frac{W_t - W_d}{W_e - W_d} \times 100 \quad (7)$$

2.3.5 Shape memory

Polymers with suitable shape memory can deform under the loading and recover their initial shape after removing the loading [57]. To measure shape memory, the deformation of cylindrical samples under compression with 200g load for 5 min was measured. The load after 5 min was

increased to 400, 600, 800, and 900 g. To examine whether the compressed hydrogels could recover the enforced deformation or not, the hydrogels under the final load were immersed in water to absorb the lost water. Then the load was decreased and deformation was recorded at the end of each interval [55].

2.3.6 In vitro degradation of hydrogel

The degradation assay was done using phosphate-buffered saline (PBS) under pH 7.4 and 37 °C. Samples were drowned in PBS, the PBS was refreshed every week and at the specified time intervals the samples were removed from immersing water and washed with DI water to remove salinity. After drying in an oven at 60 °C, samples were weighed to calculate the degradation rate using the following equation.

$$weight\ remaining\ ratio\ (WRR) = \frac{W_t}{W_0} \times 100 \qquad (8)$$

where W_t and W_0 are the hydrogel weight at specified times and the initial hydrogels weight, respectively.

2.3.7 Thermal properties

Thermal characteristics of the samples were conducted using differentiation scanning calorimetry apparatus (DSC) under the atmosphere of nitrogen. The details are available in Supporting Information.

2.3.8 Contact angle

Contact angles of hydrogels at room temperature were evaluated using OCAH 200 device (data physics contact angle system, static mode). The details are available in Supporting Information.

2.3.9 Morphology and porosity determination

Surface morphology, porous structure, and cell adhesion of the freeze-dried hydrogel were studied using scanning electron microscopy (SEM). The details are available in Supporting Information.

2.3.10 *In vitro* drug loading and drug release behavior

To evaluate the drug release behavior of the samples in stimulated and passive conditions, 50 mg of dexamethasone as drug model was dissolved in methanol, and 0.5 g of dry samples were added to the solution and stirred for 24h at ambient temperature. Then, the drug-loaded hydrogel

was washed to remove the un-bonds drugs, and the sample was immersed in PBS (pH 7.4, and 37 °C). At particular interval times, the same amount of fresh PBS was replaced. To evaluate the drug release profile, UV-Vis (λ=237 nm) was utilized. In stimulated drug release, electrical current was applied to the hydrogel and then the release pattern was determined. In order to further study of release mechanism, the Korsmeyer-Peppas exponential equation (equation (9)) was utilized [58]. The mean dissolution time (MDT) was used to evaluate the drug release rate, which was determined by Mockel and Lippold (equation (10)) [59].

$$M_t/M_f = k.t^n \quad (9)$$

$$MDT = (n/n+1).k^{-1/n} \quad (10)$$

2.3.11 Antibacterial assay

Minimum inhibitory concentration (MIC) of CAP2 for *Staphylococcus aureus* (ATCC 29213) and *Escherichia coli* (ATCC 8739) was assessed. The details are available in Supporting Information.

2.3.12 *In vitro* evaluation of hydrogel cell viability

Hydrogels biocompatibility was carried out using the MTT assay. The samples were sterilized using UV and ethanol. After sterilization, samples were washed and culture media was poured on sample overnight. Pheochromocytoma (PC12) cells in DMEM with 10% FBS were seeded on the samples and then placed in incubator (37 °C, 95% moisture, and 5% CO_2). The MTT test was performed in 1, 3, and 5 days [60].

2.3.13 Animals

Adult male Wistar rats (250-300 g) were purchased from the Pasteur Institute of Iran. They were habituated for at least 6 days in the animal facility before starting the experiments. Rats were caged in the group of four with arbitrary access to nutrients and maintained on a 12h light/dark cycle (light on at 07:00 AM) and at a temperature of 23±1 °C. We endeavored to utilize the minimum number of animals and reduce their suffering during the experiments. The experiments were performed according to the Review Board and Ethics Committee of Pasteur Institute of Iran and conform to the European Communities Council Directive of 24 November 1986 (86/609/EEC).

2.3.14 Unilateral hippocampal ischemia induction

Unilateral hippocampal ischemia was induced according to the previously described method [61, 62]. Briefly, after achieving the proper level of anesthesia using an incision in the femoral region, the femoral vein was determined and isolated from the femoral nerve and artery. Then, the distal section of the vein was strongly fastened and the proximal end was loosely tied using two pieces of thread. Using small scissors, an incision was lined on the vein to insert a polyethylene tubing (PE-50) in the femoral vein. The catheter was fixed in the vein by tightening the loose tie. In accordance with Paxinos atlas [63], a guide cannula (23 gauge stainless steel) was implanted on the upward section of the hippocampal fissure (AP= 5.64 mm, L= 5.2 mm and DV= 2.6 mm) and fixed to the skull with dental cement. To preserve a root for drugs microinjection, the cannula was sealed with a 29-gauge stainless steel stylet. After recovery, the upward section of the hippocampal fissure was illuminated by a 523 nm laser diode (CNI laser) attached to an optical fiber (200µm) for 25 min. Along the first two-minute of illumination periods, 2 mL/kg of Rose Bengal (20 mg/ml, Sigma-Aldrich Co., US) was gently injected into the femoral vein through polyethylene tube. Finally, the polyethylene tube and optical fiber were detached and the femoral region was sutured.

2.3.15 Hydrogel microinjection

The animals were randomly divided into five groups. Sham group (underwent surgery without hippocampal ischemia induction), control group (hippocampal ischemia induction plus 10 µL/rat PBS injected in the site of ischemia), hydrogel treated group (hippocampal ischemia induction plus 10 µL/rat hydrogel injected in the site of ischemia), VEGF treated group (hippocampal ischemia induction plus 10 µL/rat VEGF (1 mg/mL) injected in the site of ischemia), and hydrogel containing VEGF treated group (hippocampal ischemia induction and 10 µL/rat VEGF (1 mg/mL) loaded hydrogel injected in the site of ischemia). After animal acclimatization, the photothrombotic model was used to make unilateral selective hippocampal ischemia [64]. Three days after hippocampal ischemia induction, the stainless-steel stylet was discarded from guide cannula and the mixture was microinjected, with the rate of 1µL/min, into the ischemic site in conscious rats using a 25-µL Hamilton syringe connected a 29-gauge injection cannula through a PE-10 polyethylene tube. The volume injected was 10 µl/rat. After injection, the needle remained for 2 min in the injection site to minimize drug backflow. Infarcted volume (six rats in each

group) and behavioral evaluations (eight rats in each group) were done 5 days after drug injection.

2.3.16 Infarct volume measurement

Five days after injection, animals were sacrificed, and brains were dissected and coronally sectioned into 2-mm-thick slices using a stainless-steel brain matrix. Sliced brain sections were stained with triphenyltetrazolium chloride solution (2% in normal saline) for 20 min at 37 °C. The unstained section of the brain section was the criterion of ischemic lesions [65]. The infarct volume was quantified using the ImageJ software. The infarct volume (%) was determined using the following formula to attain the actual volume of injury [66, 67].

$$\text{Infarct volume (\%)} = \frac{\text{Volume of the left hemisphere} - \text{Non-infarct volume of the right hemisphere}}{\text{Volume of the left hemisphere}} \times 100$$

2.3.17 Behavioral testing

Memory impairment was evaluated in separate experimental groups (n=8) through passive avoidance and Morris water maze (MWM) paradigms which assessed fear-motivated memory and spatial memory performance, respectively.

2.3.18.1 Passive avoidance test

Five days after drug injection, the passive avoidance (PA) test was performed using a shuttle box equipment consisting of a bright and a dark compartment (20 cm × 20 cm × 20 cm each) floored by stainless-steel rods connecting to an electrical stimulator. A guillotine door (8 cm ×8 cm) separated the two compartments. Briefly, following two habituation sessions (30 min inter-session interval), the animals were trained to perform the task. In training trial, after entering the dark compartment the guillotine door was closed and immediately the animals were given electric foot shock (1.5 mA for 3s). Thirty seconds after applying foot shock, they were returned to the home cage. After two min, the animals were retested. They were placed in the light compartment and successful training was achieved if they did not go into the dark compartment over two min. Otherwise, training trials were repeated until the rat learned the task. Twenty-four-hour later, the animal was located in a light chamber, the guillotine door was opened and its behavior was monitored for 300s. The latency of entrance to the dark compartment known as step-through latency (STL) and total time elapsed in dark chamber (TDC) were registered.

2.3.18.2 Morris water maze test

Spatial learning and memory were assessed in the animals based on the previously described method [68]. MWM consisted of a dark water tank (155 cm) loaded with water (20 ±2 C) up to 10 cm from the tank edge. Four quadrants (North, East, West, and South) were determined for the tank using a software system (Ethovision, versionXT7, the Netherlands). A hidden stage (10 cm diameter) was positioned in the target quadrant, Q1, 1.5 cm beneath the water surface. The lab room walls were designed with specific shapes as an extra maze or spatial cues. Using a charge-coupled device (CCD) camera the swim path of animals was tracked in the pool and the locomotion was analyzed using Ethovision software 7. At first, animals were accommodated to the pool by swimming in the tank for 60 min. The platform was located in the Q1 and animals were put in the tank water from different directions to train the animals. Rats were trained for three successive days. Each day, they were trained by four trials with ten-minute inter-trial intervals. The rats were supposed to locate the hidden platform over 60s. In case the rats failed to find the platform until 60s, they were directed to it and permitted to stay there for 10s. This procedure was repeated in the second and third days. Twenty-four hours after the last session, the platform was taken out, the animal was placed in the pool from the opposite side of the platform and the motor behavior was monitored for 60s. Escape latency, distance to platform and duration in the target quadrant and swim speeds were analyzed.

2.3.18 Statistical analysis

The quantitative data were analyzed as a mean ± standard deviation. Statistical comparisons were done by using ANOVA version 16.0 (SPSS, USA). The level of significance was considered if P values were <0.05.

3. Result and discussion

3.1 Synthesis and characterization

The FTIR spectra of samples (CS, AP, CS-AP, and CAP) are illustrated in **figure 3(I)**. The spectrum of CS displays typical adsorption peaks at 3435.73 cm^{-1} related to the distinctive peak of amine (--NH_2) and hydroxyl group (--OH) stretching vibrations [69]. Peaks of 1602.27 cm^{-1} and 1423.89 cm^{-1} in CS correspond to the amide bond (--CONH--) and amine bond (--NH_2) stretching and bending vibrations. Peaks of 1081.88 cm^{-1} and 1157.82 cm^{-1} are related to pyranose (--C—O--) stretching vibrations from CS [70]. The spectrum of AP illustrates peaks at 1626.45 cm^{-1} and

1574.34 cm^{-1} due to (C==C) absorption of the benzene ring (--N—B—N) and the quinoid ring (--N==Q==N--) of AP. The 1312.06 cm^{-1} band is attributed to C—N stretching in the proximity of quinoid rings [71]. The peak at 1738.34 cm^{-1} in curve CAP is related to the C==O asymmetric stretching mode of ester in Pluronic [72]. The data confirmed the successful crosslinking and grafting reaction of the hydrogel.

3.2 Electroactivity and conductivity

Oligoanilines and polyaniline possess three oxidation states: leucoemeraldine (LE), emeraldine (EM), and pernigraniline (PN). **Figure 3(II-A)** shows the oxidation states of aniline oligomer. Polyaniline and the oligoaniline conductivity occur in the oxidation state. The UV-Vis spectra of undopped sample showed peak at 356 nm attributed to the benzene ring π-π^* transition. By doping with camphor sulfonic acid, peak at 580 nm was observed and the blue shift of benzene ring because of the polaron formation (solvantochromism effect) resulted in a peak at 338 nm **(Figure II-B)** [73-76]. Cyclic Voltammetry (CV) was used to investigate the electroactivity of hydrogels. As it is illustrated in **figure 3(II-C)**, it exhibited three pairs of quasi-reversible oxidation/reduction peaks and the mean peak potentials ($E_{1/2}$= (E_{pa} + E_{pc})/2). Peaks refer to the transition of different states of the aniline oligomer (transition between leucoemeraldine state, emeraldine state I and II, and pernigraniline state). The results indicated that the hydrogels showed good electroactivity. Also, molecular resonance is depicted in **figure 3(II-A)**. The electrochemical behavior of PC12 cells was evaluated by Kafi et al. [77]. It was observed that the PC12 cells exhibited the two redox peaks with current ratio larger than 1 which demonstrated the quasi-reversible characteristics of the cell. Hydrogel CV behavior look likes CV behavior of PC12 cell which this similarity can be inferred as an electrochemical behavior mimicking of neural cells with synthesized hydrogel.

Ionic conductivity was evaluated using four-probe method (**figure 3(III-A)**). The ionic conductivity increased by increasing the temperature due to the accelerated ionic mobility at elevated temperatures. Also, the increment of AP content enhanced the absolute conductivity because AP provided a higher number of ions for the hydrogel. According to **figure 3(III-A)** the conductivity of hydrogels at 37 °C is ca. $3*10^{-3}$ which is adequate for the cellular response (proliferation or/and differentiation) [29]. Such resemblance between the hydrogel and neural cells demonstrated the electrical mimicking of cells using synthesized hydrogel. The conductivity of hydrogels is related to two factors: the number of ions and their mobility. **Figure**

3(III-B) shows a line where the slope of the plot multiplied by R represents the activation energy for conductivity and the exponential of the intercept displays the pre-exponential factors which represents the number of ions in the hydrogel. According to equation (2), the measurements are given in Table within **figure 3-III** and it can be understood that higher pre-exponential factor and low activation energy lead to more conductivity. The pre-exponential factor increases with the increment of the AP content. Also, activation energy declines with increasing the of AP percentage in hydrogel because less conductive hydrogel required more energy for ion transfer. According to equation (3) conductivity is a subordinate of mobility and hole concentration (number of ions). With an increment of AP content, the number of ions increases. On the contrary, the higher concentration AP because of the hydrophobic nature resulted in swelling ratio decrement which restricts the mobility of ions. Thus, the conductivity of samples should be optimized in accordance with ion mobility and number. Conductivity increase with raising the AP content until an optimum point and after that, it can be deteriorated because of the hindrance effect against water molecule diffusion. Autofi et al. observed that the aniline tetramer increment enhanced the conductivity because of the enhancement of ion and mobility. After adding more aniline tetramer ionic conductivity decreased because of the less mobility of ions [55].The entire hole concentration is constant in samples with a specific AP concentration, and the increment in conductivity with temperature is due to mobility increment. On the other hand, in particular temperature, the mobility is constant. Therefore, the conductivity depends on the ion numbers [55, 56]. It has been reported that the conductive polymers affect the intracellular Ca^{2+} level of neural cells which affect their activities like proliferation and differentiation [78]. Wu et al. proposed that the CaSR-PCL pathway had more effective than voltage-gated calcium channel (VGCC) in regulating intracellular Ca^{2+} levels of neural cells on oligoaniline based conductive substrate [79]. Hence, an oligoaniline based conductive substrate can affect the signaling pathways and regulate the neural cell activities [43].

It is known that the lipid bilayer of nerve cells (the outer membrane of nerve cells with thickness around 8-10nm) performs as a leaky capacitor. Specific capacitance (capacitance per unit area of membrane) has fundamental factors in neural model which is related to signal propagation and synaptic integration. Capacitance and dendritic geometry affect the postsynaptic potential amplitude because of the depolarization of the dendritic tree at delivering the synaptic current to the membrane capacitance time interval. After that, the charge swiftly transfers from the synapse

which the speed of the signal propagation is related inversely to the capacitance. The neural cell capacitance is reported around 0.9-1.1 µF/cm2. Electrochemical impedance spectroscopy (EIS) is an outstanding method to study the cell feature and behavior using the Randles cell model which consisted of two resistances and one capacitance (**Figure 3 (IV)**). Scaffold capacitance is close to the neural capacitance which can be proper substrate for neural tissue engineering [53, 80]. Such resemblance can be declared that the scaffold can act as a bridge in the defected sites and enhance the functionality. Such resemblance declared that the synthesized hydrogel can mimic the impedance and electrochemical features of the neural tissues. Morphology, thermal properties, and contact angle of hydrogels are discussed in supplementary information (**Figure 1S-I, Figure 1S(II-A), Figure 1S(II-B) and Figure1S III, respectively**).

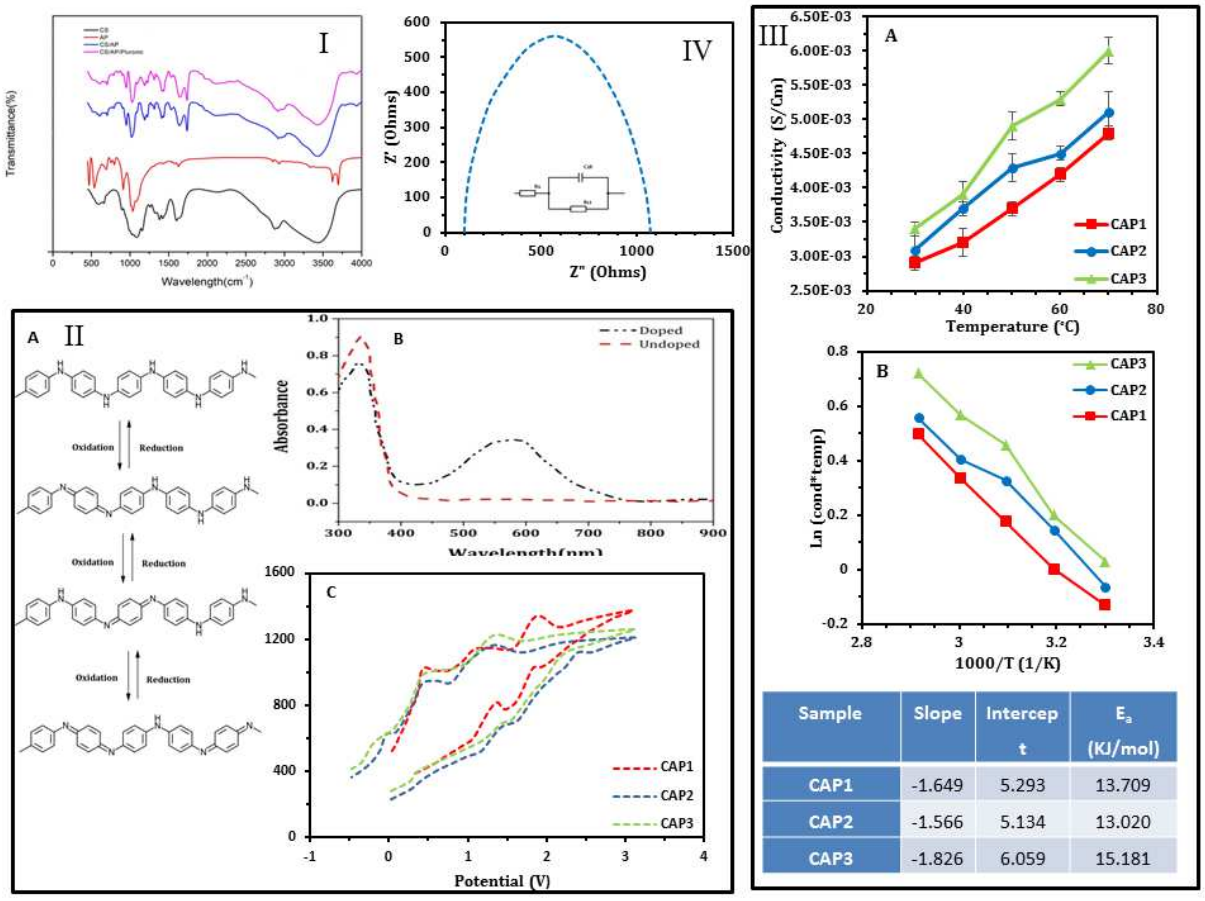

Sample	Slope	Intercept	E_a (KJ/mol)
CAP1	-1.649	5.293	13.709
CAP2	-1.566	5.134	13.020
CAP3	-1.826	6.059	15.181

Figure 3. **(I)** FTIR spectra of CS, AP, CS/AP, and CS/AP/Pluronic. **(II)** (A) The scheme of aniline pentamer transition in oxidation-reduction activities. (B) The UV spectra of hydrogels in deionized water and doped with HCl. (C) Cyclic Voltammetry of hydrogels: the sample electroactivity is featured by three oxidation/reduction peaks. **(III)** The ionic conductivity of hydrogels. Doping with camphor sulfonic acid produced emeraldine state and suitable

conductivity. (A) Conductivity against temperature and (B) Arrhenius plots of samples & table indicates the activation energy derived from the figure (B). **(IV)** Bio-impedance evaluation Nyquist plot of hydrogel which was yielded from electrochemical impedance spectroscopy that it was used for gaining the Randles circuit model components.

3.3 Rheological behavior evaluation of hydrogels

The most important factor in the injectable hydrogel is gelation time. For this, the gelation time of hydrogel was measured using the inversion method. The samples gelation was evaluated at 37°C to simulate the body temperature (**Figure 4(I)**). Gelation time was around 4, 5, and 7 minutes for CAP1, CAP2, and CAP3 samples, respectively. The gelation time increased with decreasing the Pluronic concentration in hydrogels. The amount of –CHO was increased with an increasing Pluronic concentration. Hence, CHO groups have more possibility to reaction with -NH_2 of CS to form Schiff base in the hydrogels. Moreover, Pluronic because of its nature exhibited thermosensitive gelation, decrement of Pluronic content decreased hydrogel sensitivity to temperature [81, 82]. Rheological properties are shown in **figure 4(II)**. The hydrogels with different amount of Pluronic were conducted by a time sweep experiment to evaluate the gelation process. Prompt dynamic Schiff base reaction between –CHO and –NH_2 groups resulted in rapid surpass of storage modulus from loss modulus in the initial stage [83]. The elastic modulus of hydrogels was reduced by increasing the percentage of AP because of the steric hindrance of the AP which disrupts the LCST behavior of Pluronic. The sol-gel transition of the samples can be observed in modulus versus temperature graph which indicates the thermosensitive behavior of the samples. At low temperature, G' was lower than G", indicating a viscous sol state. During the sol-gel transition, a significant increase was observed. Also with reducing the percentage of AP in samples, the gelation temperature increased [72]. Furthermore, the storage and loss modulus versus angular frequency were plotted to analyze the stability of the hydrogels. When the angular frequency altered from 0.1 rad·s^{-1} to 100 rad·s^{-1}, storage and loss modulus of hydrogel demonstrated no noteworthy changes, representing proper durability of hydrogels (**Figure 4(III)**).

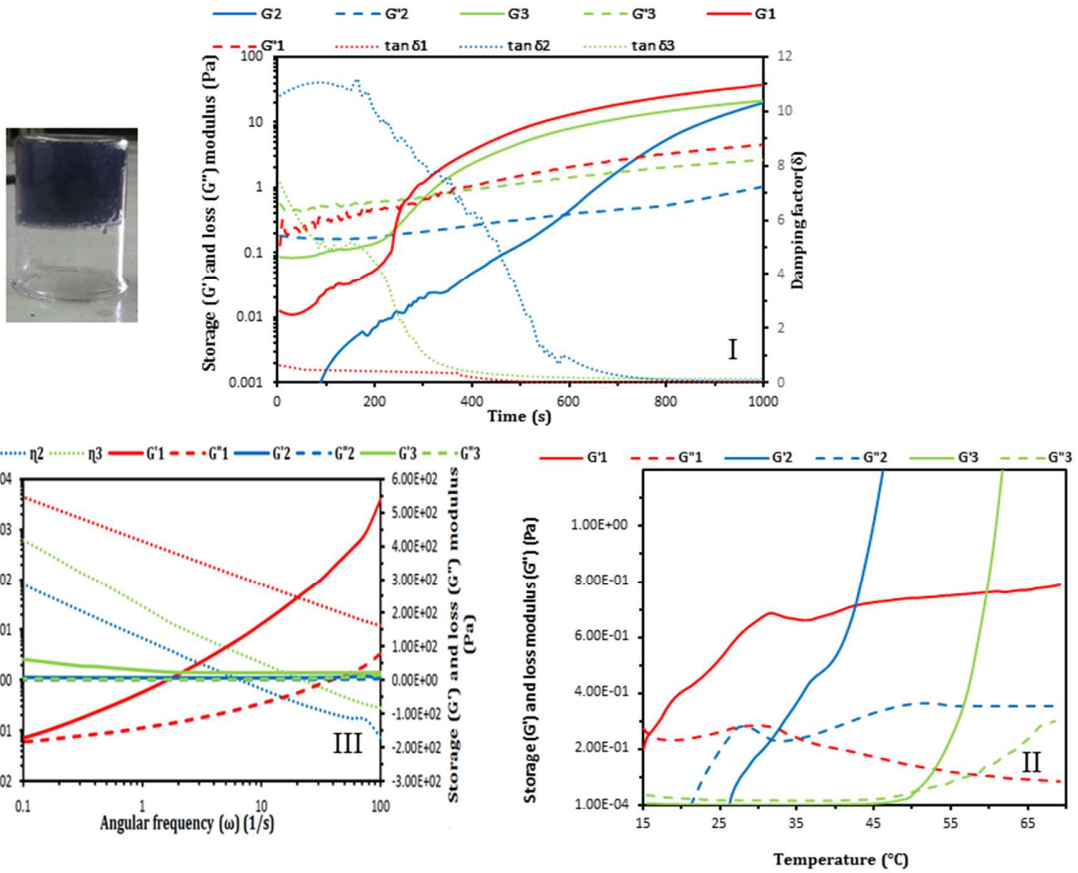

Figure 4. Photograph of hydrogel after crosslinking. (I) Rheological behavior of hydrogels in time sweep test. (II) storage (G') and loss (G") modulus of hydrogels in temperature sweep test. (III) Angular frequency sweep test.

3.4 Swelling/deswelling and hydrophilicity behavior of the hydrogels

The mechanical properties, diffusivity, and drug release of hydrogels are related to their swelling and deswelling behavior. **Figure 5(I-A)** represents the swelling ratio of hydrogels versus time at room temperature. It was obvious that the samples absorbed a high amount of water at initial time intervals and then reached an equilibrium state. During the swelling process, water molecules overcome the osmotic pressure inside the gel to permeate the gel. Elasticity force is acted against osmotic force to balance the stretching of networks to prevent the network collapse. The amount of absorbed water in the hydrogel resulted in higher elasticity and consequently higher osmotic pressure. Therefore, water needs to overcome higher pressure to permeate inside the gel. Thus, the swelling rate decreased gradually over time.

It was observed that the swelling ratio decreased with increasing the AP content in hydrogels which such a phenomenon attributed to the decrement of free space within polymeric network

hindering the diffusion of water molecules inside the hydrogel; Moreover, the hydrophobic nature of AP resulted in repulsion of water molecules. Swelling rate can be determined using rate parameter (τ) which can be obtained by rearranging the Voigt equation. The lower value of τ declares a higher the swelling rate. With plotting ln ($1-St-S_e$) versus time the slop which is $-1/\tau$ can be calculated. It was understood that the swelling ratio exhibited different behaviors during swelling time intervals which its behavior differed in the initial stage and final stage (**Figure 5(I-C,D**). The swelling rate was high at the initial stage and became low at final stage because the hydrogel reached the equilibrium swelling weight. Based on **figure 5(I-C)**, hydrogel behavior at initial time intervals obeys Voigt equation properly; however, the data in the second section does not. In the initial minutes, as the content of AP increments in the hydrogels, the slope of the trend lines decreases and the τ value increases which declared the decrement of the swelling rate. AP because of the hydrophilic nature repels the water molecules and the rate of the swelling is decreased.

The deswelling trend of hydrogels is demonstrated in **figure 5(I-B)** disclosing the fact that the amount of absorbed water by hydrogels decreases fast at the first minutes during the deswelling process, and then becomes slower until reaching the equilibrium state.

3.5 Shape memory

The result of deformation and recovery properties of hydrogels was studied. All samples recover their initial shape after they have lost amount of their water under compression which can be in accordance with the hippocampus behavior under compression test [84]. As a result, these hydrogels are suitable for use in the body due to the ability to absorb extracellular fluid (ECF) and recovering primary shape. Samples with higher AP content exhibited less compression strain (**Figure 5-II**). By increasing the percentage of AP, the rigid segments of AP limited the segmental motion and hindered movement during compression. Also, when samples recover their dismissed water, hydrogel chains retained their mobility and hold on to their initial position [55]. Based on the aforementioned results, synthesized hydrogel mimics the hippocampus mechanical behavior.

3.6 In vitro degradation assessment of hydrogels

Degradation time of hydrogels is a vital factor in tissue engineering because of the chronic inflammation happen due to the prolonged presence of the material within the body [85]. Therefore, the degradation rate of the hydrogels should be synchronized with tissue regeneration.

AP reduced swelling capacity due to its intrinsic hydrophobic properties. Hence, as the percentage of the AP in hydrogel increased, water swelling and degradation decreased (**Figure 5-III**).

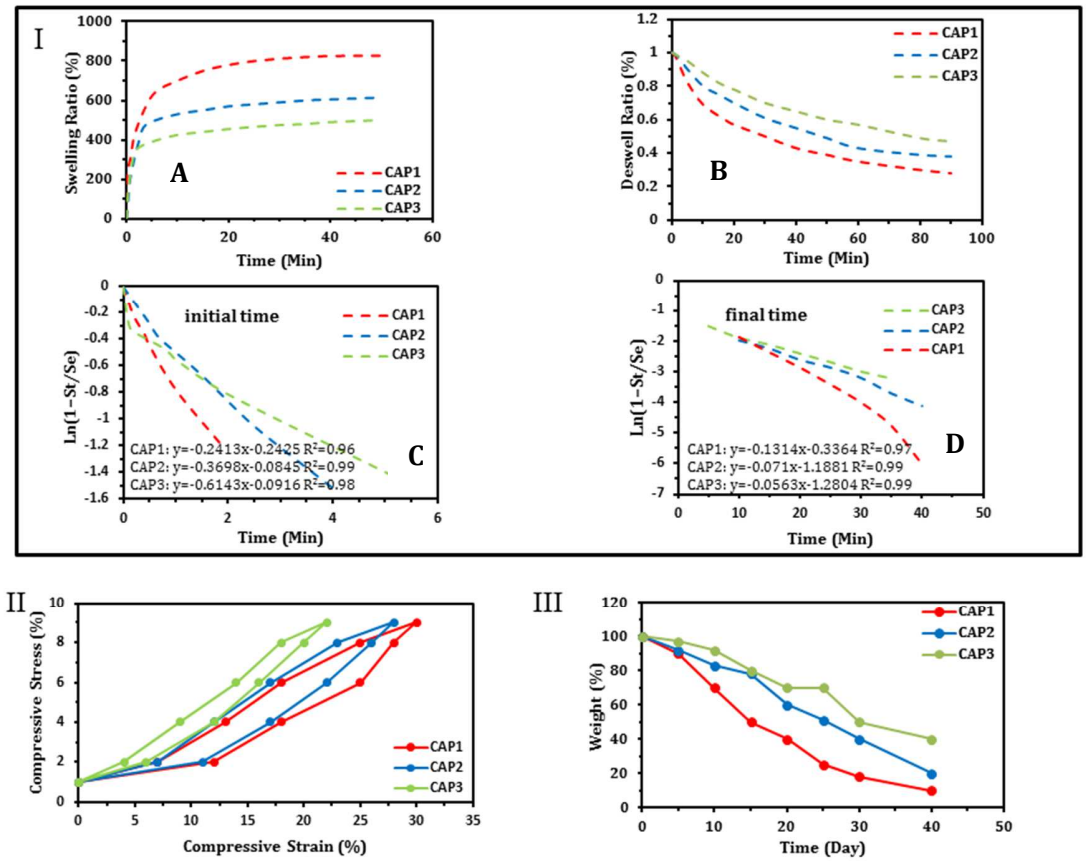

Figure 5. (I) (A) The swelling behavior of samples with various amounts of Pluronic. (B) The deswelling trend of hydrogels with various amounts of Pluronic. Ln (1−St/Se) *vs.* t for initial (C) and final (D) minutes of swelling. **(II)** Deformation and recovery of hydrogels. (**III**) Degradation profile of the hydrogels with different concentrations in PBS with pH 7.4 at 37 °C.

3.7 In vitro drug release properties of the hydrogel

Conductive hydrogels are proper platforms for the drug delivery system with on-demand electro-responsive features in which the voltage just use to promote the release of drugs [20, 86]. AP and CS can captivate drugs and interact with them by the carboxyl and amine groups via ionic interaction bonds. Besides, conductive hydrogels interact with drugs using hydrophobic, acid-base, π-π interaction, ion exchange, H-bond, and polar function. Applying electrical voltage to hydrogel generated an oxidation/reduction process and can release the drug with the desired

pattern [87, 88]. Dexamethasone in aqueous solution due to its hydrophobic nature encounters repulsion driving forces and has a tendency to be released rapidly with a high initial burst release. **Figure 6(I-A)** depicts the stimulated and passive release behavior by applying an electrical potential to the hydrogel. Conductive hydrogels were sensitive to voltage in which voltage applying resulted in increasing the drug release content due to the variation of AP's redox state. Variation causes bond cleavage in hydrogels and enhances drug release amount [89]. The first burst release of the drug-loaded CAP2 hydrogel is attributed to the drug molecules located near the surface or those loosely bond with the hydrogel. In the passive drug release, there is a direct relationship between drug release pattern and swelling/deswelling pattern, where more swelling ratio yields more drug release ratio. CAP1 because of the higher content of AP exhibited more hydrophobicity and low swelling ratio, the lower drug release from CAP1 due to the low diffusion of water molecules [90]. In electro-stimulated drug release, the release behavior of dexamethasone was determined using applying electrical stimulation to the hydrogel. Drug release mechanism in passive system was just diffusion-driven force but the electro-stimulated drug release of conductive hydrogels was attributed to the diffusion-driven force, charged molecules movement, and total net charge changing by oxidation/reduction. Oxidation is a possible mechanism for the release of positive charge drugs, conversely, drugs with negative charge are released by reduction [91]. Korsmeyer-Peppas equation is proper for evaluating drug release from CAP hydrogels with high enough correlation ($r^2 > 0.97$). It has been supposed that when the diffusion exponent (n) equal to 0.5 indicates that the release mechanism obeyed the Fickian diffusion model, and the dexamethasone was released by the Fickian diffusion [92]. The fitted data in **figure 6(I-B)** designated that CAP2 hydrogel obeys the Fickian diffusion systems and dexamethasone released by diffusion [59].

3.8 Antibacterial assay and In vitro biocompatibility

The antibacterial analysis results confirmed the successful antibacterial activity of CAP2 hydrogel against *Escherichia coli* and *Staphylococcus aureus* (**Figure 2S(I)**, Supporting Information).

The biocompatibility of hydrogel plays a key role in supporting basic cellular activities such as proliferation and adhesion. Biocompatibility and cytotoxicity were evaluated by MTT assessment with PC12 cells in various time intervals (1, 3, and 5 days). SEM images of PC12

cells seeded on CAP2 exhibited in **figure 6(II-A)** which reveals a good adhesion of cells on the scaffold. Therefore, the SEM image and MTT assessment confirmed the biocompatibility of hydrogels. Moreover, cell viability increase with time and the highest cell viability of the cell was observed after 5 days **(Figure 6(II-B))**. These properties could be attributed to the biocompatibility of CS, pluronic, and AP. On the other hand, AP has toxicity in higher concentration and affect the cellular activities inversely, therefore there is an optimum percent of AP should be determined for maximum cell proliferation. In terms of various percentages of AP, CAP2 showed the highest cell viability during the culture days which is ascribed by its swelling ratio and proper electrical/ionic conductivity.

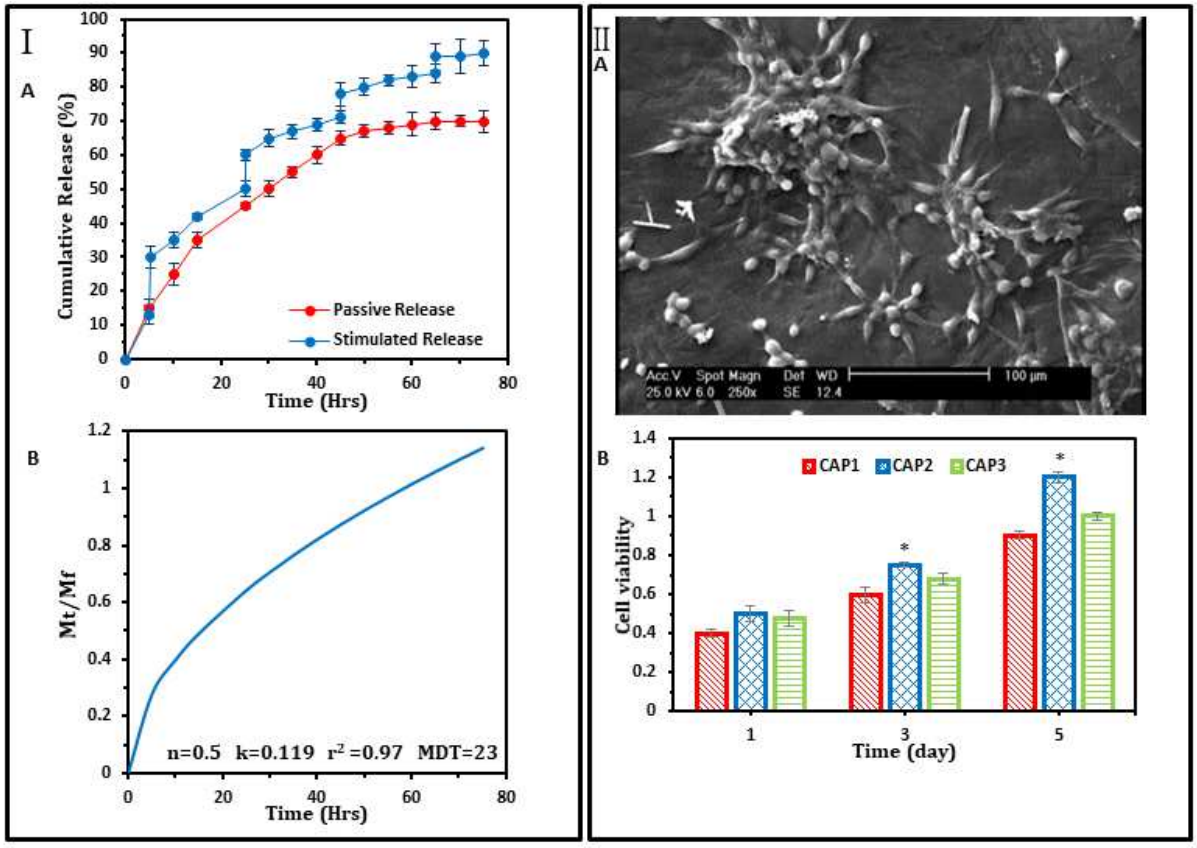

Figure 6. **(I)** Relationship between cumulative release (%) and time (hours). Passive and stimulated drug release of CAP2. (A) Electrical stimulation with various voltages results in releasing dexamethasone with the desired pattern. (B) The release profiles of CAP2 hydrogel in PBS with pH 7.4 were fitted well using Eqs. (9) and (10). **(II)** (A) SEM image of PC12 cells adhesion on CAP2, it shows that the hydrogel has the cell attachment. (B) Cell viability

test: colloidal hydrogel biocompatibility was evaluated using MTT assay with neural-like PC12 cells which the CAP2 exhibit the best cell compatibility (*P < 0.05).

4. In vivo studies

4.1 Injectable electroactive hydrogel containing VEGF decreased the infarct volume of hippocampal ischemia area

Infarct volume was assessed 5 days after drug injection using triphenyltetrazolium chloride (TTC) staining procedure. Based on **figure 7-I**, the brain infarct volume in VEGF or VEGF plus hydrogel groups was smaller in comparison with the control group (**Figure 7 (I-A)**). Quantitative data of the infarct volume was calculated using standard formula which is modified to post-ischemic edema and presented as a percentage of left hemisphere volume in **figure 7 (I-B)**. The infarcted volume in rats treated with VEGF or VEGF plus hydrogel was decreased in comparison with the control group (*** p < 0.001). Interestingly, animals treated with VEGF plus hydrogel showed less ischemic area compared with those treated with VEGF alone (# p < 0.05). There was no infarct lesion in the sham group.

4.2 Passive avoidance memory improvement by using injectable electroactive hydrogel containing VEGF

In the passive avoidance test, step-through latency (STL) intensely declined and the elapsed time in the dark compartment (TDC) intensely enhanced in the control group compared with the sham group in the retention test day (**Figure 7 (II-A)**). VEGF as a bolus injection and VEGF hydrogel both inhibited memory impairment following hippocampal ischemia as they increased the STL in passive avoidance test (* p <0.05). Furthermore, **figure 7 (II-B)** indicates that treatment with bolus injection of VEGF (* p <0.05) and VEGF hydrogel (** p <0.01) decreased time spent in a dark compartment indicating an improvement of passive avoidance memory. Interestingly, TDC in VEGF gel was significantly lower than that in animals treated with VEGF alone (# p <0.05).

4.3 Injectable electroactive hydrogel containing VEGF improved spatial learning and memory in animals suffering from selective hippocampal ischemia

Two-way ANOVA revealed a significant influence of treatment and time ($F(2, 63) = 21.03$, $P < 0.001$ and $F(4, 63) = 14.17$, $P < 0.001$, respectively) for the latency to locate the platform (escape latency) during four trials each day. Further analysis using Bonferroni posttest indicated a significant difference among sham and control (ischemic) groups ($p < 0.05$) on the second day.

On the third day, ischemic animals spent more time to find the platform in contrast to the sham group. No significant difference was detected between the control group and ischemic animals treated with hydrogel alone. However, the treatment of ischemic animals with VEGF alone ($p < 0.05$) and VEGF loaded hydrogel ($p < 0.001$) resulted in improved escape latency compared to the control group (**Figure. 7(II-A)**). Distance to the platform is another parameter to analyze the animal's behavior to know how far they have swum from the platform. Two-way ANOVA followed by Bonferroni posttest revealed significant difference between sham and control group in the consecutive days (1st,2nd and 3rd days, $p < 0.01$, $p < 0.001$ and $p < 0.001$, respectively), indicating that the control group swam farther away from the platform and showed impaired acquisition of the task. No difference was found between the control group and animals treated with hydrogel alone. However, treatment ischemic animals with VEGF hydrogel led to swim closer to the platform in the first and third days ($p < 0.05$ and $p < 0.001$, respectively) in comparison with the control group. VEGF alone improved the performance on the third day ($p < 0.05$) in contrast to the control group (**Figure 7 (III-A and B)**).

Twenty-four h after training, the platform was taken out and animals were permitted to swim for 60 s. The statistical analysis declared that the control group elapsed less time in the target quadrant compared to the sham group ($p < 0.001$), indicating that hippocampal ischemia caused to impaired spatial memory performance (**Figure 7 (IV-A)**). Treatment with hydrogel could not rescue the spatial memory function. However, treatment with VEGF alone and VEGF loaded hydrogel reversed impaired spatial memory toward the sham level. Intriguingly, animals treated with VEGF hydrogel showed better performance compared with those treated with VEGF alone (**Figure 7 (IV-A)**, $p < 0.05$).

Animals with hippocampal ischemia have also swum farther from the platform position, indicating that they failed to recall the task comparing to the sham group (**Figure 7 (IV-B)**, $p < 0.001$). Also, they showed less number of entries into the target quadrant in the test day compared to the sham group (**Figure 7 (IV-C)**). While treatment with the scaffold alone did not change the performance, VEGF containing hydrogel decreased the distance to the platform and increased the number of the entrance to the target quadrant in comparison with the control group ($p < 0.01$ and $p < 0.05$, respectively). VEGF hydrogel group swam closer to the platform compared to the animals treated with VEGF alone ($p < 0.05$).

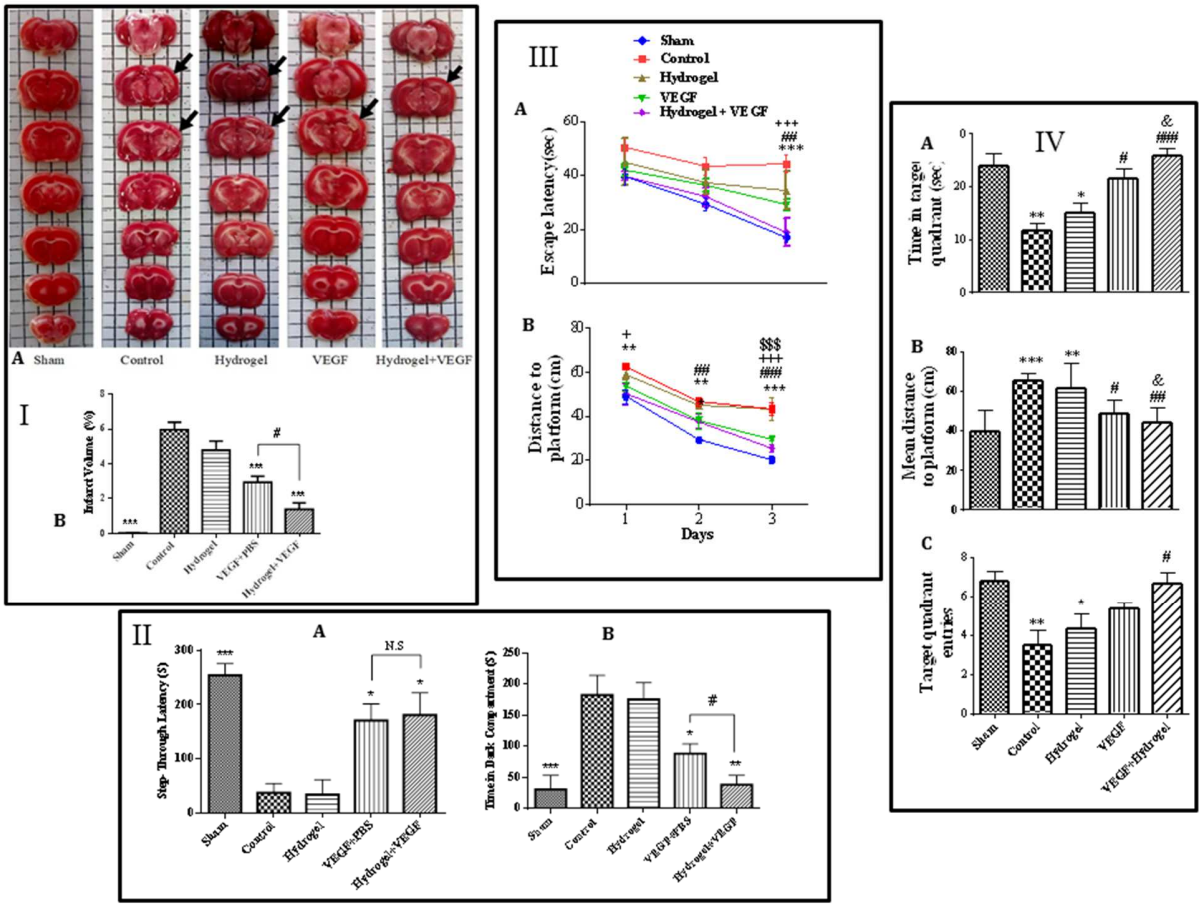

Figure 7. (I) VEGF loaded hydrogel decreased the infarct size in animals suffering from selective hippocampal ischemia. Five days after drug microinjection, coronal brain slices were prepared and stained with TTC. The unstained areas of the brain slice were defined as ischemic lesions. (B) The percentage of actual infarct volume in the left hemisphere volume. The infarct volume was significantly increased in the control group compared with the sham group (***p < 0.001). However, treatment with VEGF and hydrogel containing VEGF treated groups decreased the infarct size in contrast to the control group (*** p <0.001). No infarction was found in the hippocampus of sham group. Animals treated with VEGF hydrogel showed lesser infarct volume compared with the VEGF treated group (#p < 0.05). All values were expressed as mean ± SEM (n=6) .**(II)** VEGF hydrogel rescued animals with hippocampal ischemia more efficiently from avoidance memory impairment. (A) Step-Through Latency (STL) at the retention test day in passive avoidance test. Animals in the sham, VEGF and hydrogel containing VEGF treated groups had more latency to enter the dark compartment compared with the control group (* p < 0.05 and *** p < 0.001). (B) Time in the dark compartment (TDC) at the retention test day in passive avoidance test. Animals in the sham, VEGF and hydrogel containing VEGF treated groups spend less time in the dark compartment compared with control group (* p < 0.05, ** p < 0.01 and *** p < 0.001). VEGF treated animals spent less time in the dark compartment compared with the VEGF group (# p <0.05). All values were expressed as mean ± SEM (n=6-7). **(III)** Microinjection of VEGF hydrogel into the hippocampus improves acquisition of spatial tasks in animals suffering from the hippocampal ischemia. All animals were trained in three consecutive days. (A) Animals with hippocampal ischemia spent more time to locate platform in the tank compared to the sham group (***p < 0.001). Microinjection of scaffold hydrogel did not improve the performance. However, treatment with hydrogel containing VEGF decrease the time to find the platform compared to the control group (+++p < 0.001).

##p<0.01 the sham group compared to the hydrogel group. (B) Induction of hippocampal infarction resulted in swimming farther from platform compared to the sham group. However, microinjection of hydrogel loaded VEGF into the infarcted hippocampus decreased the path swimming distance to the platform. All values were expressed as mean ± SEM (n=6-8). ** p < 0.01 and *** p < 0.001 comparing the sham and control groups. ##p < 0.01 and ###p < 0.001 comparing sham and hydrogel groups. +p < 0.05 and +++p < 0.001 comparing control and VEGF loaded hydrogel groups. $$$p < 0.001 comparing hydrogel and hydrogel containing VEGF groups. **(IV)** Treatment with VEGF hydrogel improved spatial memory function in animals with hippocampal infarction. (A) Animals hippocampal ischemia spent less time in the target quadrant compared with the sham group. However, treatment of ischemic animals with VEGF alone and hydrogel containing VEGF reverse the spatial memory toward sham group. (B) Induction of hippocampal ischemia resulted in swimming farther from the platform in control group compared to the sham group. Treatment with VEGF and hydrogel containing VEGF both decreased the distance to the platform. However, VEGF hydrogel group showed less swimming distance to the platform compared to the VEGF group. (C) The number of entrance into the target quadrant was significantly decreased in the control group compared to the sham group and treatment with hydrogel containing VEGF restored it toward the sham group. * p < 0.05, ** p < 0.01 and *** p < 0.001 comparing with sham group. All values were expressed as mean ± SEM (n=6-8). # p < 0.05, ## p < 0.01 and ### p < 0.001 comparing with control group. & p < 0.05 comparing to VEGF group.

5. Conclusion

In the present study we designed a brain compatible hydrogel which mimics the electrical, electrochemical, and mechanical features of the hippocampus. Hydrogel was synthesized based on CS-aniline pentamer/Pluronic in which Pluronic endows the injectability feature to the hydrogel. Moreover, aniline pentamers endow the electroactivity along with antibacterial properties. CS has been selected due to its antibacterial and ECM-like properties. FTIR approved the hydrogel formation. Cyclic voltammetry and four probe method have been utilized to measure the electroactivity and conductivity, respectively. The conductivity of samples was similar to the brain tissue which can mimic the electrical properties of brain tissue. Mechanical properties of samples were evaluated by rheometry measurement which was accommodated with brain tissue. Moreover, the rheometry test proved the injectability properties. The AP enhanced the hydrogel thermal stability as confirmed by using DSC and TGA. We have shown that sustained release of VEGF in electroconductive hydrogel delivering system restored histological and behavioral consequences of focal cerebral ischemia. The results revealed that the infarcted size in VEGF hydrogel-treated rats was decreased more than 70 % compared to the ischemic (control) group. Behavioral tests confirmed the comparable beneficial effect of sustained delivery of VEGF on hippocampal dependent learning and memory performance. In almost all tests, sustained release of VEGF showed superior beneficial effects rather than VEGF alone. The hippocampal injuries resulted in different dysfunctions ranging from cognitive deficit to epilepsy, and multiple methods have been suggested for the regeneration of ischemic

hippocampus. Miscellaneous materials have been tested for regeneration of hippocampal neurons following ischemia. In the present study, a novel biocompatible conductive injectable hydrogel has been designed and examined on the rat model of ischemia induced in the hippocampus. VEGF is the main regulator of angiogenesis which has been reported that is strongly up-regulated within the penumbra (ischemic border). In addition, VEGF receptors have been shown to up-regulated at the border after two days and later in the ischemic core [93], indicating its important action on restoring tissue homeostasis after injuries. In consistent with our data multiple studies showed that VEGF may have potential therapeutic role in neuronal surveillance in brain injuries [93-96]. However, its short half-life and poor accessibility to the desired cerebral regions after peripheral administration limit its potential. Our injectable VEGF delivery system may provide continuous, dose-controlled delivery for long lasting time, controllable dosage, and capability of direct administration of VEGF at the site of injury. We found the protective effect of VEGF in young rat model of cerebral ischemia. Attention should be taken that stroke is usually occur in elderly individuals in which poor resilience impede the recovery of neural structure and function following injury [97, 98]. They also have different microenvironment and neuroinflammatory state rather than young individuals [99, 100]. Further study in old animal models may be required to address this issue.

Disclosure statement

No potential conflict of interest was reported by the authors.

References

[1] M. Koehl and D. N. Abrous, "A new chapter in the field of memory: adult hippocampal neurogenesis," *European Journal of Neuroscience,* vol. 33, pp. 1101-1114, 2011.

[2] H. Toyoda, X.-Y. Li, L.-J. Wu, M.-G. Zhao, G. Descalzi, T. Chen*, et al.*, "Interplay of amygdala and cingulate plasticity in emotional fear," *Neural plasticity,* vol. 2011, 2011.

[3] F. Stella, E. Cerasti, B. Si, K. Jezek, and A. Treves, "Self-organization of multiple spatial and context memories in the hippocampus," *Neuroscience & Biobehavioral Reviews,* vol. 36, pp. 1609-1625, 2012.

[4] L. Kartsounis, P. Rudge, and J. Stevens, "Bilateral lesions of CA1 and CA2 fields of the hippocampus are sufficient to cause a severe amnesic syndrome in humans," *Journal of Neurology, Neurosurgery & Psychiatry,* vol. 59, pp. 95-98, 1995.

[5] L. Peng and M. A. Bonaguidi, "Function and dysfunction of adult hippocampal neurogenesis in regeneration and disease," *The American journal of pathology,* 2017.

[6] C. G. Wible, "Hippocampal physiology, structure and function and the neuroscience of schizophrenia: a unified account of declarative memory deficits, working memory deficits and schizophrenic symptoms," *Behavioral Sciences,* vol. 3, pp. 298-315, 2013.
[7] H. Jun, S. Mohammed Qasim Hussaini, M. J. Rigby, and M.-H. Jang, "Functional role of adult hippocampal neurogenesis as a therapeutic strategy for mental disorders," *Neural plasticity,* vol. 2012, 2012.
[8] Z. Zhou, P. Yu, H. M. Geller, and C. K. Ober, "The role of hydrogels with tethered acetylcholine functionality on the adhesion and viability of hippocampal neurons and glial cells," *Biomaterials,* vol. 33, pp. 2473-2481, 2012.
[9] R. Alizadeh, P. Zarrintaj, S. K. Kamrava, Z. Bagher, M. Farhadi, F. Heidari*, et al.*, "Conductive hydrogels based on agarose/alginate/chitosan for neural disorder therapy," vol. 224, p. 115161, 2019.
[10] M. Farokhi, F. Mottaghitalab, M. A. Shokrgozar, D. L. Kaplan, H.-W. Kim, and S. C. Kundu, "Prospects of peripheral nerve tissue engineering using nerve guide conduits based on silk fibroin protein and other biopolymers," *International Materials Reviews,* vol. 62, pp. 367-391, 2017.
[11] A. Subramanian, U. M. Krishnan, and S. Sethuraman, "Development of biomaterial scaffold for nerve tissue engineering: Biomaterial mediated neural regeneration," *Journal of biomedical science,* vol. 16, p. 108, 2009.
[12] Z. Bagher, Z. Atoufi, R. Alizadeh, M. Farhadi, P. Zarrintaj, L. Moroni*, et al.*, "Conductive hydrogel based on chitosan-aniline pentamer/gelatin/agarose significantly promoted motor neuron-like cells differentiation of human olfactory ecto-mesenchymal stem cells," vol. 101, pp. 243-253, 2019.
[13] N. A. Peppas and J. J. Sahlin, "Hydrogels as mucoadhesive and bioadhesive materials: a review," *Biomaterials,* vol. 17, pp. 1553-1561, 1996.
[14] A. Hejčl, P. Lesný, M. Přádný, J. Michalek, P. Jendelova, J. Štulík*, et al.*, "Biocompatible hydrogels in spinal cord injury repair," *Physiol Res,* vol. 57, pp. S121-S132, 2008.
[15] Y. Zhong and R. V. Bellamkonda, "Biomaterials for the central nervous system," *Journal of the Royal Society Interface,* vol. 5, pp. 957-975, 2008.
[16] M. Servatan, P. Zarrintaj, G. Mahmodi, S.-J. Kim, M. R. Ganjali, M. R. Saeb*, et al.*, "Zeolites in drug delivery: progress, challenges and opportunities," 2020.
[17] S. M. H. Dabiri, A. Lagazzo, F. Barberis, M. Farokhi, E. Finochio, and L. Pastorino, "Characterization of alginate-brushite in-situ hydrogel composites," *Materials Science and Engineering: C,* vol. 67, pp. 502-510, 2016.
[18] F. Avani, S. Damoogh, F. Mottaghitalab, A. Karkhaneh, and M. Farokhi, "Vancomycin loaded halloysite nanotubes embedded in silk fibroin hydrogel applicable for bone tissue engineering," *International Journal of Polymeric Materials and Polymeric Biomaterials,* vol. 69, pp. 32-43, 2020.
[19] D. Zhang, F. Di, Y. Zhu, Y. Xiao, and J. Che, "Electroactive hybrid hydrogel: Toward a smart coating for neural electrodes," *Journal of Bioactive and Compatible Polymers,* vol. 30, pp. 600-616, 2015.
[20] P. Zarrintaj, S. Manouchehri, Z. Ahmadi, M. R. Saeb, A. M. Urbanska, D. L. Kaplan*, et al.*, "Agarose-based biomaterials for tissue engineering," *Carbohydrate polymers,* 2018.
[21] R. Khalili, P. Zarrintaj, S. H. Jafari, H. Vahabi, and M. R. J. I. J. o. B. M. Saeb, "Electroactive poly (p-phenylene sulfide)/r-Graphene Oxide/Chitosan as a novel potential candidate for tissue engineering," 2020.
[22] R. Balint, N. J. Cassidy, and S. H. Cartmell, "Conductive polymers: towards a smart biomaterial for tissue engineering," *Acta biomaterialia,* vol. 10, pp. 2341-2353, 2014.

[23] A. Saberi, F. Jabbari, P. Zarrintaj, M. R. Saeb, and M. J. B. Mozafari, "Electrically Conductive Materials: Opportunities and Challenges in Tissue Engineering," vol. 9, p. 448, 2019.
[24] C. L. Weaver, J. M. LaRosa, X. Luo, and X. T. Cui, "Electrically controlled drug delivery from graphene oxide nanocomposite films," *ACS nano,* vol. 8, pp. 1834-1843, 2014.
[25] V. Pillay, T. S. Tsai, Y. E. Choonara, L. C. du Toit, P. Kumar, G. Modi*, et al.*, "A review of integrating electroactive polymers as responsive systems for specialized drug delivery applications," *Journal of Biomedical Materials Research Part A,* vol. 102, pp. 2039-2054, 2014.
[26] A. Samadi, R. Hasanzadeh, T. Azdast, H. Abdollahi, P. Zarrintaj, and M. R. J. J. o. M. S. Saeb, Part B, "Piezoelectric Performance of Microcellular Polypropylene Foams Fabricated Using Foam Injection Molding as a Potential Scaffold for Bone Tissue Engineering," pp. 1-14, 2020.
[27] P. B. Milan, S. Khamseh, P. Zarrintaj, B. Ramezanzadeh, M. Badawi, S. Morisset*, et al.*, "Copper-enriched diamond-like carbon coatings promote regeneration at the bone–implant interface," *Heliyon,* vol. 6, p. e03798, 2020/04/01/ 2020.
[28] W.-C. Huang, H. S. Wu, and C. J. Bettinger, "Materials and microfabrication processes for next-generation brain-machine devices," *SPIE Newsroom,* 2016.
[29] M. Akhtari, D. Emin, B. Ellingson, D. Woodworth, A. Frew, and G. Mathern, "Measuring the local electrical conductivity of human brain tissue," *Journal of Applied Physics,* vol. 119, p. 064701, 2016.
[30] P. Zarrintaj, Z. Ahmadi, H. Vahabi, F. Ducos, M. R. Saeb, and M. Mozafari, "Polyaniline in retrospect and prospect," *Materials Today: Proceedings,* vol. 5, pp. 15852-15860, 2018.
[31] J. Hu, L. Huang, X. Zhuang, P. Zhang, L. Lang, X. Chen*, et al.*, "Electroactive aniline pentamer cross-linking chitosan for stimulation growth of electrically sensitive cells," *Biomacromolecules,* vol. 9, pp. 2637-2644, 2008.
[32] G. Sargazi, D. Afzali, A. Mostafavi, A. Shadman, B. Rezaee, P. Zarrintaj*, et al.*, "Chitosan/polyvinyl alcohol nanofibrous membranes: towards green super-adsorbents for toxic gases," vol. 5, p. e01527, 2019.
[33] A. Rastegari, F. Mottaghitalab, and M. Farokhi, "Fabrication Technology of Chitosan-Based IPN: Drug Delivery Application," in *Interpenetrating Polymer Network: Biomedical Applications*, ed: Springer, 2020, pp. 55-78.
[34] S. Mohebbi, M. N. Nezhad, P. Zarrintaj, S. H. Jafari, S. S. Gholizadeh, M. R. Saeb*, et al.*, "Chitosan in biomedical engineering: a critical review," vol. 14, pp. 93-116, 2019.
[35] B. Bagheri, P. Zarrintaj, A. Samadi, R. Zarrintaj, M. R. Ganjali, M. R. Saeb*, et al.*, "Tissue engineering with electrospun electro-responsive chitosan-aniline oligomer/polyvinyl alcohol," 2020.
[36] M. Koosha, H. Mirzadeh, M. A. Shokrgozar, and M. Farokhi, "Nanoclay-reinforced electrospun chitosan/PVA nanocomposite nanofibers for biomedical applications," *RSC Advances,* vol. 5, pp. 10479-10487, 2015.
[37] S. Manouchehri, B. Bagheri, S. H. Rad, M. N. Nezhad, Y. C. Kim, O. O. Park*, et al.*, "Electroactive bio-epoxy incorporated chitosan-oligoaniline as an advanced hydrogel coating for neural interfaces," vol. 131, pp. 389-396, 2019.
[38] P. Zarrintaj, H. Vahabi, M. R. Saeb, and M. Mozafari, "Application of polyaniline and its derivatives," in *Fundamentals and Emerging Applications of Polyaniline*, ed: Elsevier, 2019, pp. 259-272.
[39] B. Bagheri, P. Zarrintaj, S. S. Surwase, N. Baheiraei, M. R. Saeb, M. Mozafari*, et al.*, "Self-gelling electroactive hydrogels based on chitosan–aniline oligomers/agarose for neural tissue engineering with on-demand drug release," vol. 184, p. 110549, 2019.
[40] M. Gajendiran, J. Choi, S.-J. Kim, K. Kim, H. Shin, H.-J. Koo*, et al.*, "Conductive biomaterials for tissue engineering applications," vol. 51, pp. 12-26, 2017.

[41] M. K. Yazdi, H. Saeidi, P. Zarrintaj, M. R. Saeb, and M. Mozafari, "PANI-CNT nanocomposites," in *Fundamentals and Emerging Applications of Polyaniline*, ed: Elsevier, 2019, pp. 143-163.
[42] P. Zarrintaj, R. Khalili, H. Vahabi, M. R. Saeb, M. R. Ganjali, and M. Mozafari, "Polyaniline/metal oxides nanocomposites," in *Fundamentals and Emerging Applications of Polyaniline*, ed: Elsevier, 2019, pp. 131-141.
[43] P. Zarrintaj, B. Bakhshandeh, M. R. Saeb, F. Sefat, I. Rezaeian, M. R. Ganjali*, et al.*, "Oligoaniline-based conductive biomaterials for tissue engineering," *Acta biomaterialia,* 2018.
[44] Z. Ahmadi, N. P. S. Chauhan, P. Zarrintaj, A. B. Khiabani, M. R. Saeb, and M. Mozafari, "Experimental procedures for assessing electrical and thermal conductivity of polyaniline," in *Fundamentals and Emerging Applications of Polyaniline*, ed: Elsevier, 2019, pp. 227-258.
[45] N. Hassani Besheli, S. Damoogh, B. Zafar, F. Mottaghitalab, H. Motasadizadeh, F. Rezaei*, et al.*, "Preparation of a codelivery system based on vancomycin/silk scaffold containing silk nanoparticle loaded VEGF," *ACS Biomaterials Science & Engineering,* vol. 4, pp. 2836-2846, 2018.
[46] M. Farokhi, F. Mottaghitalab, J. Ai, and M. A. Shokrgozar, "Sustained release of platelet-derived growth factor and vascular endothelial growth factor from silk/calcium phosphate/PLGA based nanocomposite scaffold," *International journal of pharmaceutics,* vol. 454, pp. 216-225, 2013.
[47] H. Basiri, A. Abouei Mehrizi, A. Ghaee, M. Farokhi, M. Chekini, and E. Kumacheva, "Carbon dots conjugated with vascular endothelial growth factor for protein tracking in angiogenic therapy," *Langmuir,* vol. 36, pp. 2893-2900, 2020.
[48] Y. Sun, K. Jin, L. Xie, J. Childs, X. O. Mao, A. Logvinova*, et al.*, "VEGF-induced neuroprotection, neurogenesis, and angiogenesis after focal cerebral ischemia," *The Journal of clinical investigation,* vol. 111, pp. 1843-1851, 2003.
[49] R. Langer and M. Moses, "Biocompatible controlled release polymers for delivery of polypeptides and growth factors," *Journal of cellular biochemistry,* vol. 45, pp. 340-345, 1991.
[50] D. F. Emerich, E. Silva, O. Ali, D. Mooney, W. Bell, S. J. Yu*, et al.*, "Injectable VEGF hydrogels produce near complete neurological and anatomical protection following cerebral ischemia in rats," *Cell Transplantation,* vol. 19, pp. 1063-1071, 2010.
[51] L. Chen, Y.-H. Yu, H.-P. Mao, X.-F. Lu, W.-J. Zhang, and Y. Wei, "Synthesis of amino-capped aniline pentamer and UV-Vis spectral study," *CHEMICAL JOURNAL OF CHINESE UNIVERSITIES-CHINESE EDITION-,* vol. 25, pp. 1768-1770, 2004.
[52] R. Dong, X. Zhao, B. Guo, and P. X. Ma, "Biocompatible elastic conductive films significantly enhanced myogenic differentiation of myoblast for skeletal muscle regeneration," *Biomacromolecules,* vol. 18, pp. 2808-2819, 2017.
[53] P. Zarrintaj, B. Bakhshandeh, I. Rezaeian, B. Heshmatian, and M. R. Ganjali, "A novel electroactive agarose-aniline pentamer platform as a potential candidate for neural tissue engineering," *Scientific reports,* vol. 7, p. 17187, 2017.
[54] K. Lee, S. Cho, S. H. Park, A. Heeger, C.-W. Lee, and S.-H. Lee, "Metallic transport in polyaniline," *Nature,* vol. 441, p. 65, 2006.
[55] Z. Atoufi, P. Zarrintaj, G. H. Motlagh, A. Amiri, Z. Bagher, and S. K. Kamrava, "A novel bio electro active alginate-aniline tetramer/agarose scaffold for tissue engineering: synthesis, characterization, drug release and cell culture study," *Journal of Biomaterials Science, Polymer Edition,* vol. 28, pp. 1617-1638, 2017.
[56] W. Zhao, L. Glavas, K. Odelius, U. Edlund, and A.-C. Albertsson, "Facile and green approach towards electrically conductive hemicellulose hydrogels with tunable conductivity and swelling behavior," *Chemistry of Materials,* vol. 26, pp. 4265-4273, 2014.
[57] M. Xie, L. Wang, J. Ge, B. Guo, and P. X. Ma, "Strong electroactive biodegradable shape memory polymer networks based on star-shaped polylactide and aniline trimer for bone tissue engineering," *ACS applied materials & interfaces,* vol. 7, pp. 6772-6781, 2015.

[58] J. Qu, X. Zhao, P. X. Ma, and B. Guo, "pH-responsive self-healing injectable hydrogel based on N-carboxyethyl chitosan for hepatocellular carcinoma therapy," *Acta biomaterialia,* vol. 58, pp. 168-180, 2017.
[59] J. E. Möckel and B. C. Lippold, "Zero-order drug release from hydrocolloid matrices," *Pharmaceutical research,* vol. 10, pp. 1066-1070, 1993.
[60] A. Nemati, M. Saghafi, S. Khamseh, E. Alibakhshi, P. Zarrintaj, and M. R. Saeb, "Magnetron-sputtered Ti x N y thin films applied on titanium-based alloys for biomedical applications: Composition-microstructure-property relationships," *Surface and Coatings Technology,* 2018.
[61] S. M. Hosseini, H. G. Pourbadie, M. Sayyah, M. I. Zibaii, and N. J. B. b. r. Naderi, "Neuroprotective effect of monophosphoryl lipid A, a detoxified lipid A derivative, in photothrombotic model of unilateral selective hippocampal ischemia in rat," vol. 347, pp. 26-36, 2018.
[62] S. M. Hosseini, H. G. Pourbadie, N. Naderi, M. Sayyah, M. I. J. J. o. p. Zibaii, and t. methods, "Photothrombotically induced unilateral selective hippocampal ischemia in rat," vol. 94, pp. 77-86, 2018.
[63] G. Paxinos, "C. Watson C:"The rat brain in stereotaxic coordinates, Ed 6"," ed: Academic Press, 2007.
[64] S. M. Hosseini, H. G. Pourbadie, N. Naderi, M. Sayyah, and M. I. Zibaii, "Photothrombotically induced unilateral selective hippocampal ischemia in rat," *Journal of pharmacological and toxicological methods,* 2018.
[65] F. Hua, J. Ma, T. Ha, J. L. Kelley, R. L. Kao, J. B. Schweitzer*, et al.*, "Differential roles of TLR2 and TLR4 in acute focal cerebral ischemia/reperfusion injury in mice," *Brain research,* vol. 1262, pp. 100-108, 2009.
[66] Y. Ji, Y. Hu, Y. Wu, Z. Ji, W. Song, S. Wang*, et al.*, "Therapeutic time window of hypothermia is broader than cerebral artery flushing in carotid saline infusion after transient focal ischemic stroke in rats," *Neurological research,* vol. 34, pp. 657-663, 2012.
[67] Y.-B. Ji, P.-P. Zhuang, Z. Ji, Y.-M. Wu, Y. Gu, X.-Y. Gao*, et al.*, "TFP5 peptide, derived from CDK5-activating cofactor p35, provides neuroprotection in early-stage of adult ischemic stroke," *Scientific reports,* vol. 7, p. 40013, 2017.
[68] H. Gholamipour-Badie, N. Naderi, F. Khodagholi, F. Shaerzadeh, and F. Motamedi, "L-type calcium channel blockade alleviates molecular and reversal spatial learning and memory alterations induced by entorhinal amyloid pathology in rats," *Behavioural brain research,* vol. 237, pp. 190-199, 2013.
[69] J. Hu, L. Huang, X. Zhuang, X. Chen, Y. Wei, and X. Jing, "A new oxidation state of aniline pentamer observed in water-soluble electroactive oligoaniline-chitosan polymer," *Journal of Polymer Science Part A: Polymer Chemistry,* vol. 46, pp. 1124-1135, 2008.
[70] L. Zhang, Y. Li, L. Li, B. Guo, and P. X. Ma, "Non-cytotoxic conductive carboxymethyl-chitosan/aniline pentamer hydrogels," *Reactive and Functional Polymers,* vol. 82, pp. 81-88, 2014.
[71] C. Luo, H. Peng, L. Zhang, G.-L. Lu, Y. Wang, and J. Travas-Sejdic, "Formation of nano-/microstructures of polyaniline and its derivatives," *Macromolecules,* vol. 44, pp. 6899-6907, 2011.
[72] E. Jin, Z. Zhang, H. Lian, X. Chen, C. Xiao, X. Zhuang*, et al.*, "Injectable electroactive hydrogels based on Pluronic® F127 and tetraaniline copolymer," *European Polymer Journal,* vol. 88, pp. 67-74, 2017.
[73] H. Cui, Y. Liu, Y. Cheng, Z. Zhang, P. Zhang, X. Chen*, et al.*, "In vitro study of electroactive tetraaniline-containing thermosensitive hydrogels for cardiac tissue engineering," *Biomacromolecules,* vol. 15, pp. 1115-1123, 2014.

[74] P. Zarrintaj, M. K. Yazdi, M. Jouyandeh, and M. R. Saeb, "Chapter 7 - PANI-based nanostructures," in *Fundamentals and Emerging Applications of Polyaniline*, M. Mozafari and N. P. S. Chauhan, Eds., ed: Elsevier, 2019, pp. 121-130.
[75] M. R. Saeb, P. Zarrintaj, P. Khandelwal, and N. P. S. Chauhan, "Synthetic route of polyaniline (I): Conventional oxidative polymerization," in *Fundamentals and Emerging Applications of Polyaniline*, ed: Elsevier, 2019, pp. 17-41.
[76] M. R. Saeb and P. Zarrintaj, "Chapter 10 - Polyaniline/graphene-based nanocomposites," in *Fundamentals and Emerging Applications of Polyaniline*, M. Mozafari and N. P. S. Chauhan, Eds., ed: Elsevier, 2019, pp. 165-175.
[77] M. A. Kafi, T.-H. Kim, C.-H. Yea, H. Kim, and J.-W. Choi, "Effects of nanopatterned RGD peptide layer on electrochemical detection of neural cell chip," *Biosensors and Bioelectronics,* vol. 26, pp. 1359-1365, 2010.
[78] J. Huang, Z. Ye, X. Hu, L. Lu, and Z. Luo, "Electrical stimulation induces calcium-dependent release of NGF from cultured Schwann cells," *Glia,* vol. 58, pp. 622-631, 2010.
[79] Y. Wu, L. Wang, B. Guo, Y. Shao, and P. X. Ma, "Electroactive biodegradable polyurethane significantly enhanced Schwann cells myelin gene expression and neurotrophin secretion for peripheral nerve tissue engineering," *Biomaterials,* vol. 87, pp. 18-31, 2016.
[80] L. J. Gentet, G. J. Stuart, and J. D. Clements, "Direct measurement of specific membrane capacitance in neurons," *Biophysical journal,* vol. 79, pp. 314-320, 2000.
[81] P. Zarrintaj, Z. Ahmadi, M. R. Saeb, and M. Mozafari, "Poloxamer-based stimuli-responsive biomaterials," *Materials Today: Proceedings,* vol. 5, pp. 15516-15523, 2018.
[82] P. Zarrintaj, M. Jouyandeh, M. R. Ganjali, B. S. Hadavand, M. Mozafari, S. S. Sheiko*, et al.*, "Thermo-sensitive polymers in medicine: A review," 2019.
[83] L. Li, J. Ge, B. Guo, and P. X. Ma, "In situ forming biodegradable electroactive hydrogels," *Polymer Chemistry,* vol. 5, pp. 2880-2890, 2014.
[84] J. Van Dommelen, T. Van der Sande, M. Hrapko, and G. Peters, "Mechanical properties of brain tissue by indentation: interregional variation," *Journal of the mechanical behavior of biomedical materials,* vol. 3, pp. 158-166, 2010.
[85] M. Sarem, F. Moztarzadeh, M. Mozafari, and V. P. Shastri, "Optimization strategies on the structural modeling of gelatin/chitosan scaffolds to mimic human meniscus tissue," *Materials Science and Engineering: C,* vol. 33, pp. 4777-4785, 2013.
[86] B. Bakhshandeh, P. Zarrintaj, M. O. Oftadeh, F. Keramati, H. Fouladiha, S. Sohrabi-jahromi*, et al.*, "Tissue engineering; strategies, tissues, and biomaterials," *Biotechnology and Genetic Engineering Reviews,* vol. 33, pp. 144-172, 2017.
[87] M. C. Klak, E. Lefebvre, L. Rémy, R. Agniel, J. Picard, S. Giraudier*, et al.*, "Gelatin-Alginate Gels and Their Enzymatic Modifications: Controlling the Delivery of Small Molecules," *Macromolecular bioscience,* vol. 13, pp. 687-695, 2013.
[88] T.-G. Kim, C. Kim, and J.-W. Park, "Redox-Responsive Self-Assembly of Amphiphilic Multiblock Rod–Coil Polymers," *Macromolecules,* vol. 50, pp. 8185-8191, 2017.
[89] H. Kim, S.-M. Jeong, and J.-W. Park, "Electrical switching between vesicles and micelles via redox-responsive self-assembly of amphiphilic rod− coils," *Journal of the American Chemical Society,* vol. 133, pp. 5206-5209, 2011.
[90] N. Mac Kenna, P. Calvert, A. Morrin, G. G. Wallace, and S. E. Moulton, "Electro-stimulated release from a reduced graphene oxide composite hydrogel," *Journal of Materials Chemistry B,* vol. 3, pp. 2530-2537, 2015.
[91] J. Qu, X. Zhao, P. X. Ma, and B. Guo, "Injectable antibacterial conductive hydrogels with dual response to an electric field and pH for localized “smart” drug release," *Acta biomaterialia,* vol. 72, pp. 55-69, 2018.

[92] Y. Ren, X. Zhao, X. Liang, P. X. Ma, and B. Guo, "Injectable hydrogel based on quaternized chitosan, gelatin and dopamine as localized drug delivery system to treat Parkinson's disease," *International journal of biological macromolecules,* vol. 105, pp. 1079-1087, 2017.
[93] H. J. Marti, M. Bernaudin, A. Bellail, H. Schoch, M. Euler, E. Petit*, et al.*, "Hypoxia-induced vascular endothelial growth factor expression precedes neovascularization after cerebral ischemia," *The American journal of pathology,* vol. 156, pp. 965-976, 2000.
[94] T. Hayashi, K. Abe, and Y. Itoyama, "Reduction of ischemic damage by application of vascular endothelial growth factor in rat brain after transient ischemia," *Journal of Cerebral Blood Flow & Metabolism,* vol. 18, pp. 887-895, 1998.
[95] A. Zhang, L. Liang, H. Niu, P. Xu, and Y. Hao, "Protective effects of VEGF treatment on focal cerebral ischemia in rats," *Molecular medicine reports,* vol. 6, pp. 1315-1318, 2012.
[96] M. Sondell, G. Lundborg, and M. Kanje, "Vascular endothelial growth factor has neurotrophic activity and stimulates axonal outgrowth, enhancing cell survival and Schwann cell proliferation in the peripheral nervous system," *Journal of Neuroscience,* vol. 19, pp. 5731-5740, 1999.
[97] A. Popa-Wagner, I. Dinca, S. Yalikun, L. Walker, H. Kroemer, and C. Kessler, "Accelerated delimitation of the infarct zone by capillary-derived nestin-positive cells in aged rats," *Current neurovascular research,* vol. 3, pp. 3-13, 2006.
[98] A. Popa-Wagner, S. T. Carmichael, Z. Kokaia, C. Kessler, and L. C. Walker, "The response of the aged brain to stroke: too much, too soon?," *Current Neurovascular Research,* vol. 4, pp. 216-227, 2007.
[99] R. E. Sandu, A. T. Balseanu, C. Bogdan, M. Slevin, E. Petcu, and A. Popa-Wagner, "Stem cell therapies in preclinical models of stroke. Is the aged brain microenvironment refractory to cell therapy?," *Experimental gerontology,* vol. 94, pp. 73-77, 2017.
[100] A.-M. Buga, M. Di Napoli, and A. Popa-Wagner, "Preclinical models of stroke in aged animals with or without comorbidities: role of neuroinflammation," *Biogerontology,* vol. 14, pp. 651-662, 2013.